

now published as: D. Vanzo, M. Ricci, R. Berardi, C. Zannoni, *Soft Matter*, 8, 11790-11800 (2012)

Shape, chirality and internal order of freely-suspended nematic nanodroplets

Davide Vanzo,^a Matteo Ricci,^a Roberto Berardi^a and Claudio Zannoni^{*a}

version: Tuesday 11 September, 2012

Received Xth XXXXXXXXXXXX 2012, Accepted Xth XXXXXXXXXXXX 20XX

First published on the web Xth XXXXXXXXXXXX 200X

DOI: 10.1039/b000000x

We investigate the properties of freely-suspended nematic nanodroplets of increasing size formed by elongated Gay-Berne mesogens, using extensive molecular dynamics simulations. We find that the nanodroplets have an elongated shape with an aspect ratio changing with size and that in the 50–100 nm size range ($N \approx 50,000$ – $100,000$ particles) they show a spontaneous symmetry breaking of the surface bipolar director field into a twisted pattern, whose chirality we quantify with a specific index. The droplets are found to be inhomogeneous in terms, *e.g.* of the local orientational order, and a detailed description of their internal and interfacial structure is given.

1 Introduction

The condensation of a vapour can lead to the formation of freely suspended liquid droplets whose shape is spherical for a normal isotropic liquid, as long as gravity effects are negligible. The spherical shape, as known since the work of Lord Rayleigh over a century ago¹, results from the balance of the surface free energy $\mathcal{F}_\sigma = \text{surface area} \times \sigma$, depending in turn on the surface tension σ , and the bulk free energy \mathcal{F}_V proportional to the droplet volume. The characterisation and prediction of droplet shapes for micrometric sizes and below is now very important in ink-jet technology where they are used not only for standard ink printing, but also to deliver controlled picolitre quantities of some functional material, *e.g.* an organic semiconductor, in a precise position over a surface as required in a variety of organic electronics applications^{2,3}.

Liquid crystals (LC) are important examples of those modern functional materials and have been proposed for applications going from organic field effect transistors (OFET) to organic photovoltaics (OPV) where their ability to yield molecular organisations that couple fluidity (and thus defects and annealing potential) and long-range order (*e.g.* to improve charge carrier mobility over isotropic materials) is particularly appealing (see, *e.g.*⁴).

Apart from the rather large, micron size droplets, either freely suspended or dispersed in a liquid or polymer matrix^{5,6}, much smaller liquid or liquid crystal droplets, in the range of 50–500 nm, thus with volumes between

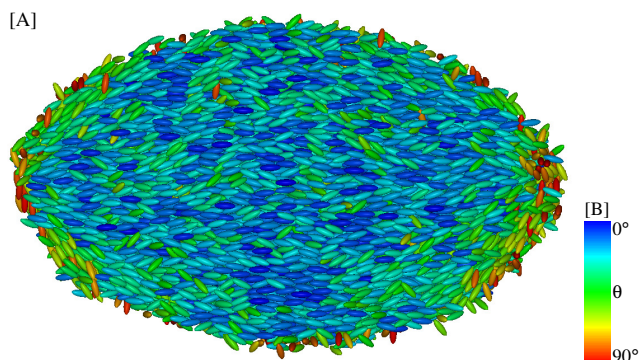


Fig. 1 View of the longitudinal cross section of an equilibrated freely-suspended nematic droplet of size $N \approx 47,000$ at $T^* = 0.53$ in equilibrium with its vapour at $\langle P^* \rangle = 0.0005 \pm 0.0004$ after 9×10^6 MD time steps (plate A). The GB particles have been colour coded according to their orientation θ with respect to principal inertia axis of the droplet (plate B). For clarity the GB particles in the surrounding vapour phase are not shown.

femtolitres and attolitres can now be prepared and studied^{7,8}, and are expected to be important in the fabrication of nanodevices. In particular micro and nano size nematic droplets are most promising for biosensor applications^{9–11}.

It should be observed that the liquid crystal droplets we are interested in here have various differences with respect to isotropic ones in that: (i) their shape is not necessarily spherical as the surface tension of liquid crystals is anisotropic and an anchoring energy term^{12,13} contributes to the free energy balance (ii) the molecular or-

^a Dipartimento di Chimica Fisica e Inorganica, Università di Bologna, Bologna, Italy, Fax: +39 051 2093690; Tel: +39 051 2097012; E-mail: claudio.zannoni@unibo.it

ganisation at the droplet surface is certainly not easy to predict and can vary from radial to tangential, or to other more complex ones (iii) the droplet interior can be non-homogeneous, *e.g.* in terms of the local order^{5,6}.

The external shape aspect of LC droplets has been studied for a long time, at least for “large” micrometric size droplets in suspensions. Important milestones in this field were the experiments of Bernal and Fanckuchen¹⁴ leading to the observation of elongated spindle-like shaped droplets, or micelles, formed by colloidal aqueous suspensions of tobacco mosaic virus particles, and of Zoher¹⁵ reporting the formation of similar aggregates in colloidal lyotropic LC of inorganic rod-shaped vanadium pentoxide particles followed by many others more recently^{16–19}.

These elongated aggregates called *tactoids* have a three dimensional shape ideally obtained by the revolution of an arc of a circle around its chord. They are obtained when the constituent particles are tangential to the boundary and are endowed with topological point defects (also called *boojums*²⁰) of the (bipolar) director field at their sharp apices.

All these observations were reported for lyotropic systems (even though as diverse as virus suspensions and chromonic systems), where the aggregates stand in an isotropic medium, but similar behaviour has also been found for thermotropic mesogens²¹.

Dispersions of droplets of micro (PDLC) or even of nano (holographic PDLC, H-PDLC) size in polymeric matrices^{22,23} or encapsulated in a polymer capsule²⁴, all cases where of course the droplet shape is fixed, can also be obtained by suitable polymerisation.

From the theoretical point of view the modelling of the equilibrium shape and director distribution in tactoidal nematic droplets has been built up and refined over the years by various authors and in particular Herring²⁵, Chandrasekhar²⁶, Williams²⁷, Huang²⁸ and Virga²⁹. Frank’s elastic continuum theory³⁰ and Wulff construction²⁶ have been employed to predict equilibrium shapes showing that they can vary from lenticular or regular with a continuous director field without disclinations to tactoid as the ratio between the anisotropic to isotropic contribution to the Rapini anchoring energy¹² varies from negative to greater than one²⁹. The role of anchoring energy on tactoids has also been discussed¹⁸ and their topological defects studied^{31,32}.

Even for the simpler spherical shape LC droplets can provide surprising effects. Thus, Volovik and Lavrentovich³¹ observed spherical droplets where the director field lines connecting the two poles rather than being simple arcs (meridians), *i.e.* bipolar structures, showing only splay and bend, were instead twisted, making the

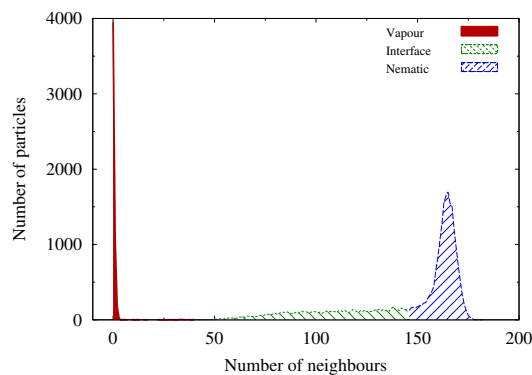


Fig. 2 Population histogram of GB particles with a given number of neighbours within a $5\sigma_0$ distance from their centre for the equilibrated nanodroplet of Figure 1. The bins corresponding to the vapour, the interface, and the bulk nematic phase have been filled respectively as solid red, and green and blue hatch patterns with different orientations. The thresholds used to identify the vapour and the nematic are respectively 40 and 145 neighbours (see text).

droplet chiral. Williams²⁷ put forward the theoretical prediction that a spontaneous chiral symmetry breaking with the onset of a twisted director configuration should occur in spherical droplets of achiral mesogens with tangential boundary conditions when the splay, twist and bend LC elastic constants (K_{11} , K_{22} , K_{33}) obey the inequality $K_{11} \geq K_{22} + 0.43K_{33}$ ^{5,27}.

Chiral droplets were actually experimentally obtained, in agreement with this predictions, by Lavrentovich and Sergan³³ and Xu, Kitzerow and Crooker³⁴.

Prinsen and van der Schoot^{35,36} have extended the model of Williams²⁷ by allowing the LC droplet to have a non-spherical shape (*e.g.* elongated) and the director field to be not perfectly bipolar. By introducing an anchoring parameter they predicted a variety of transitions between homogeneous, bipolar and twisted nematic configurations, occurring upon changing size at certain critical droplet volumes. Recently Tortora and Lavrentovich³⁷ have demonstrated and explained the origin of a spontaneous chiral symmetry breaking into *loxodromes* (*i.e.* surface director patterns intersecting the droplet meridians at constant angle) in micrometric tactoid droplets of chromonic liquid crystals deposited on a flat surface from aqueous solutions.

Overall the problem of droplet shape and director configuration seems to be well handled at continuum theory level for micron size droplets. However, it is worth noting that as the droplet size shrinks to the nanolevel the applicability of continuum type theories, and of their top-down predictions, becomes less obvious or even ques-

tionable.

Here, we take a different, complementary, approach and consider the formation of the LC droplet from the molecular level up, without assuming *a priori* the validity of continuum elastic equations, but rather hoping to test their applicability which is, it should be said, often amazingly good even on the nano-range^{13,38}.

From this point of view computer simulations provide us with a powerful and reliable way to investigate the formation and the evolution of LC nanodroplets in various conditions and allow a direct analysis of the ordering inside them. The advantage of computer simulations is that they do not require a prior knowledge or an assumption about the mesoscopic material properties like (anisotropic) surface tension or elastic constants, since these quantities collectively emerge in the simulated sample from the properties of the underlying pair potential between the constituent particles. This direct approach turns out to be also an advantage because the calculation from computer simulations of the mesoscopic material properties (*e.g.* elastic constants^{39–45}, flexoelectric coefficients⁴⁶, or surface tension^{47–50}) which constitute the input parameters of the continuum models and theories is not straightforward because of its slow convergence, and it is subject to large statistical errors. Moreover, the surface tension calculation presents an added difficulty arising from the necessity of extending the available algorithms (*e.g.* see refs.^{47–51}), originally devised for planar or spherical interfaces, to more complex and *a priori* unknown geometries.

Computer simulations have been previously performed on micro/nanodroplets typically confined by a dense medium, *e.g.* for studying the orientational order and defects of micrometric liquid crystal droplets^{52–54} embedded in a solid (typically a polymer) matrix (PDLC and H-PDLC) and thus with a fixed volume and shape.

Different methodologies and models have also been used. Thus, in one approach, Lebwohl–Lasher type lattice models, where molecules (or groups of molecules) are represented by a vector (“spin”) positioned at the sites of a cubic lattice, have been used to study the orientational order, director distribution and topological defects inside spherical nematic droplets with different boundary conditions (radial, bipolar, etc.)^{55–57}, also in the presence of external fields⁵⁶.

While the previous works assume a certain droplet shape and boundary condition, an anisotropic lattice gas spin model has been used by Bates⁵⁸ to study with Monte Carlo simulations the shape of nematic microdroplets.

Another mesoscopic technique employed has been dissipative particle dynamics (DPD), where a single nanodroplet formed by mesogens constituted of sticky

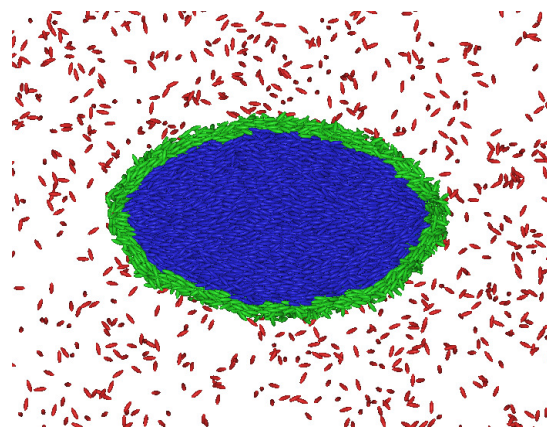


Fig. 3 View of the longitudinal cross section view of a freely-suspended nematic nanodroplet, and surrounding vapour, showing the mapping of GB particles into vapour (red), nematic (blue), and interface (green) as described in the text and in the legend of Figure 2.

spheres chains connected by springs and confined inside a spherical regions has been simulated to study the effect of an external field on a LC droplet⁵⁹.

Off-lattice models of Gay–Berne (GB) ellipsoids⁶⁰, or hard spherocylinders⁶¹ confined to spherical pores have also been studied. de Pablo and coworkers^{54,62,63} have recently used molecular dynamics to study the changes of molecular organisation taking place in a spherical GB droplet when changing the anchoring strength and its direction with respect to the surface. These effects are becoming very important for visualising through simple polarised optical investigations the presence or not of analytes in a suspension of LC microdroplets, with obvious applications for sensors.

Considering off-lattice atomistic or molecular models without the constraint of fixed shape, or confinement an early study of freely-suspended nematic droplets in vacuum⁶⁴ was performed using an atomistic model of 5CB (4'-n-pentyl-4-cyanobiphenyl) to create aggregates of 26 and 50 nematic molecules. At the time of the work a validated force field for 5CB, able to reproduce its bulk properties⁶⁵ was not available. Moreover the very small number of particles forming these droplets, more comparable to the size of a nucleation centre than to a stable liquid nanodroplet, does not really allow to compare the simulation results with theories. The limitation on sample size when dealing with atomistic models is still significant nowadays, given that current sample sizes for systems of this complexity are rarely beyond a few thousand molecules¹³.

Larger sample sizes can be studied with molecular resolution models where each molecule is replaced by a sim-

ple object endowed with certain interactions, like the attractive–repulsive Gay–Berne ellipsoids^{60,66–71} or hard spherocylinders^{72,73}.

The formation of LC nanodroplet emulsions by phase separation from a homogeneous solution of Gay–Berne mesogens ($N_{GB} = 200, 300, 400$) of 3 : 1 *length-to-width* ratio in an isotropic solvent ($N_{LJ} = 5000 - N_{GB}$ Lennard–Jones spherical particles) has been studied by us⁷⁴ and extended by Brown *et al.*⁷⁵. Also in this case deviations of the LC droplet *length-to-width* aspect ratio from spherical have been observed and the internal order described.

A Monte Carlo simulation of aggregates of 200–700 hard elongated spherocylinders (aspect ratio of 11 : 1) at different osmotic pressures has been performed by Trukhina *et al.*⁷⁶, finding that at sufficiently high osmotic pressure, elongated nematic droplets are formed with a uniform director field for the smaller ones and a bipolar structure for the larger.

Very recently Rull, Romero–Enrique and Fernandez–Nieves⁷⁷ have used Monte Carlo simulations for studying the effect of molecular elongation, *i.e.* *length-to-width* ratios 3 : 1, 4 : 1, and 6 : 1 on the shape anisotropy of freely–suspended Gay–Berne nematic nanodroplets in coexistence with their vapour. They found that the particles aligned tangentially at the surface and along the main axis of the drop, and that increasing the aspect ratio the shape of the drop becomes singular in the vicinity of the defects, and there is a crossover to an almost homogeneous texture. In this case the effect of droplet size was not investigated and the total number of Gay–Berne particles, including the coexisting vapour was $N_{GB} = 4000$.

We notice that in all the off–lattice simulation studies of freely suspended droplets a relatively small number of particles was investigated and that the peculiar switch to chiral structures predicted by theory³⁵ for sufficiently large droplets was never observed. The theoretical expectations are in any case that the chiral structure is not likely to appear for droplet formed by rigid rod-like particles and that some degree of flexibility may be required³⁵.

The aim of the present work is that of addressing the issues of nanodroplet shape and chirality, obtaining via coarse–grained molecular dynamics (MD) simulations a molecular level description of the self–organisation process and the structural characterisation of freely–suspended nematic nanodroplets in equilibrium with their vapour. We will investigate size dependent effects for droplet size more than an order of magnitude larger than current ones⁷⁷ reaching sizes that in real units would be of the order of tens of nanometres and compare these MD results with the available experimental findings and theoretical predictions. We have used the Gay–Berne

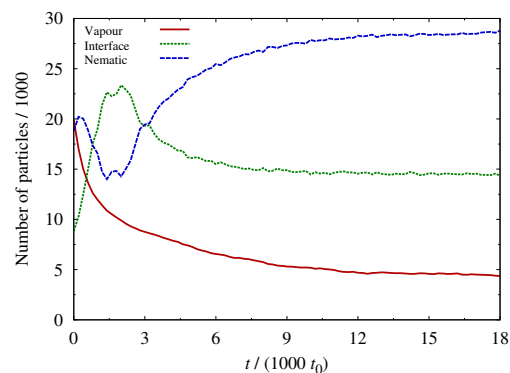


Fig. 4 Initial evolution of the populations for the vapour (red, continuous curve), interface (green, dotted curve), and nematic (blue, dashed curve) regions during the equilibration at $T^* = 0.53$ for the nanodroplet with $N \approx 47,000$ (see Figure 1). Time is measured in $t_0 = (\epsilon_0^{-1} \sigma_0^2 m_0)^{1/2}$ units.

pair potential^{66,74,78,79} and performed molecular dynamics (MD) simulations, rather than Monte Carlo, so as to be able to follow the time evolution of aggregate formation.

In particular, we have focused on determining the structure of the nematic–vapour interface, the director distribution, and the possibility of observing a spontaneous chiral symmetry breaking in a freely–suspended nematic nanodroplet of achiral mesogenic particles. More specifically, the plan of this paper is the following: in Section 2 we present the pair potential model and the technical details of the molecular dynamics simulations. The Section 3 describes the procedure devised for preparing the starting MD samples and their subsequent equilibration towards stable freely–suspended nematic nanodroplets in equilibrium with their vapour. The analysis of the properties and structure of these aggregates of various number of particles is discussed in Section 4. A Conclusions section closes the paper.

2 Model and technical details

As already mentioned, we have chosen to model our mesogenic molecules at coarse–grained level with the uniaxial Gay–Berne pair potential^{66,70,71}, an anisotropic generalisation of the venerable Lennard–Jones model where the interaction between two ellipsoids with axes $\sigma_x = \sigma_y < \sigma_z$ and interaction strengths $\epsilon_x = \epsilon_y > \epsilon_z$ is written as

$$U_{GB}(\mathbf{r}, \hat{\mathbf{u}}_1, \hat{\mathbf{u}}_2) = 4 \epsilon_0 \epsilon(\hat{\mathbf{r}}, \hat{\mathbf{u}}_1, \hat{\mathbf{u}}_2) \times [u^{12}(\mathbf{r}, \hat{\mathbf{u}}_1, \hat{\mathbf{u}}_2) - u^6(\mathbf{r}, \hat{\mathbf{u}}_1, \hat{\mathbf{u}}_2)]. \quad (1)$$

In particular, the shifted term $u(\mathbf{r}, \hat{\mathbf{u}}_1, \hat{\mathbf{u}}_2) \equiv \sigma_c / (r - \sigma(\hat{\mathbf{r}}, \hat{\mathbf{u}}_1, \hat{\mathbf{u}}_2) + \sigma_c)$ depends on the centre–centre distance r , modulus of the intermolecular vector $\mathbf{r} = \mathbf{r}_2 - \mathbf{r}_1 = r \hat{\mathbf{r}}$ and the anisotropic function $\sigma(\hat{\mathbf{r}}, \hat{\mathbf{u}}_1, \hat{\mathbf{u}}_2)$ approximating the contact distance between two ellipsoids^{80,81} having orientations of their $D_{\infty h}$ axes defined by the unit vectors $\hat{\mathbf{u}}_i$ and centre of mass at $\mathbf{r}_i = (x_i, y_i, z_i)$. The contact function depends on the orientations and on $\hat{\mathbf{r}}$ and it is parameterised with respect to the *length-to-width* ratio $\kappa = \sigma_z/\sigma_x$. The anisotropic interaction function $\epsilon(\hat{\mathbf{r}}, \hat{\mathbf{u}}_1, \hat{\mathbf{u}}_2)$ scales the amplitude of the U_{GB} pair potential, and it is parameterised in terms of κ , and on the additional coefficient $\kappa' = \epsilon_z/\epsilon_x$ defining the ratio between the *end-to-end* and *side-by-side* well depth energies^{78,79}. In addition, the empirical parameters σ_c , μ , and ν allow to tune the width and depth of these attractive wells.

The molecular units of length σ_0 , energy ϵ_0 , and mass m_0 have been used to define the dimensionless values of energy $U^* = U/U_0 = U/\epsilon_0$, temperature $T^* = T/T_0 = T/(k_{\text{B}}^{-1}\epsilon_0)$, pressure $P^* = P/P_0 = P/(\sigma_0^{-3}\epsilon_0)$, number density $\rho^* = \rho/\rho_0 = \sigma_0^3 N/V$, and time $t^* = t/t_0 = t/(\epsilon_0^{-1}\sigma_0^2 m_0)^{1/2}$. All physical observables have been computed in dimensionless form, and to compare them with real units we can take as references the width, the energy (in terms of the $k_{\text{B}}T_{\text{NI}}$ isotropic–nematic transition temperature), and the mass relative to the 4′-n-octyl-4-cyanobiphenyl (8CB) mesogen. This choice corresponds to $\sigma_0 = 5 \times 10^{-10}$ m, $\epsilon_0 = 1.4 \times 10^{-21}$ J, and $m_0 = 4.8 \times 10^{-22}$ kg. The derived units of time and pressure are instead $t_0 = 3 \times 10^{-10}$ s, and $P_0 = 112$ bar.

We have relied on previous simulation works^{60,67} to choose a parameterisation for the GB potential and thermodynamic simulation conditions providing a nematic phase coexisting in equilibrium with its vapour: using as parameters $\kappa = \sigma_z/\sigma_x = 3$, $\kappa' = \epsilon_z/\epsilon_x = 1.25$, $\sigma_c = 1 \sigma_0$, $\mu = 2$, $\nu = 1$, and mass $m^* = m/m_0 = 1.5$. The dimensionless bulk transition temperatures between the crystal, nematic and isotropic phases for this model are respectively $T_{\text{CN}}^* = 0.50$ and $T_{\text{NI}}^* = 0.54$ ^{60,67}. This parameterisation is also interesting because it leads to a tangential orientation of the mesogens at the nematic–vapour interface, as shown in⁶⁰, thus realising one of the basic conditions leading to bipolar and possibly twisted structures.

All MD simulations were run at constant volume and temperature using the weak–coupling algorithm due to Berendsen⁸², and a dimensionless time step $\Delta t^* = \Delta t/t_0 = 0.002$. To choose an optimal value for the GB potential cutoff r_c we ran preliminary constant volume and temperature MD simulations of an $N = 10,000$ spherical isotropic droplet at equilibrium with its vapour using cutoff radii ranging from $4 \sigma_0$ to $8 \sigma_0$. Eventually, the GB cutoff $r_c = 5 \sigma_0$ was chosen since it gives aver-

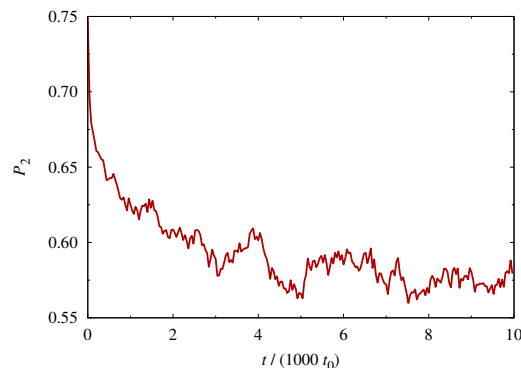


Fig. 5 Time evolution of the instantaneous overall order parameter P_2 for the nematic nanodroplet with $N \approx 47,000$ (see Figure 1). Data points have been sampled every 20 time steps from a MD run 5×10^6 time steps long. Time is measured in $t_0 = (\epsilon_0^{-1}\sigma_0^2 m_0)^{1/2}$ units.

age potential energies within 2–3% from those obtained with larger r_c values, and it provides the same thermodynamic behaviour (at least far from phase transition temperatures) without increasing unnecessarily the computational toll. It should be noticed that with this choice of r_c our phase space points do not exactly match any longer those of de Miguel *et al.*⁶⁷ who used the lower cutoff value $r_c = 4 \sigma_0$; furthermore the curved droplet interface also determines an additional term in the hydrostatic pressure of the nematic phase arising from Laplace’s contribution. However, as discussed in the next Section, these small differences have not greatly affected the behaviour of our GB droplets with respect to the phase diagram of de Miguel *et al.*, at least in the nematic region used to perform our MD simulations.

The simulations were ran using as parallel MD engine the program LAMMPS^{83,84}. In particular, we have performed all calculations using hybrid CPU/GPU architectures based on the NVIDIA Tesla graphic processors and the CUDA programming framework⁸⁵.

3 Samples preparation and equilibration

In this section we describe the procedure followed for preparing freely–suspended nematic nanodroplets in equilibrium with their vapour: an aggregate with size $N \approx 47,000$ GB particles will be used to discuss the specific details, while the results for the larger droplets are presented in the next section.

The nanodroplet preparation procedure started from a bulk nematic sample of $N = 27,000$ GB particles simulated at constant dimensionless temperature $T^* = 0.53$, and pressure $P^* = 0.0003$, in a cubic box and with fully

periodic boundary conditions in the three-dimensions. After an equilibration of 5×10^5 time steps, the sample attained an average number density $\langle \rho^* \rangle = \sigma_0^3 N \langle 1/V \rangle = 0.297$ and an orientational order parameter $\langle P_2 \rangle = 0.75$, which considering the effect of the cutoff radius discussed earlier, are in good agreement with the published bulk values reported by de Miguel *et al.*⁶⁷ and Emerson, Faetti and Zannoni⁶⁰. The dimensionless temperature $T^* = 0.53$ is close to the published phase boundary between nematic and isotropic fluids, and was chosen on purpose to reduce the probability of observing the formation either of a surface-induced or a Laplace's pressure-induced smectic ordering into the sessile nanodroplet. The cubic nematic sample was then inserted at the centre of a larger orthogonal simulation box with sides five times larger than those of the liquid crystalline aggregate (*i.e.* $L_x = L_y = L_z = 160.6 \sigma_0$). The volume not occupied by the nematic sample was filled with a supersaturated GB vapour previously equilibrated at temperature $T^* = 0.53$ and number density $\rho^* = 0.003$. To remove any possible correlation arising from this preparation procedure, and prior to starting the MD evolution of the two-phase system, we randomly sampled linear and angular momenta of both vapour and nematic particles from uniform distributions at $T^* = 0.53$. The ensuing MD equilibration of 9×10^6 time steps was performed under periodic boundaries at constant volume and temperature as described before. The average dimensionless pressure for the whole sample (*i.e.* both vapour and droplet GB particles) calculated during the equilibration run was $\langle P^* \rangle = 0.0005 \pm 0.0004$.

In the course of the equilibration the nematic aggregate underwent a relevant size increase (due to a considerable surface condensation of particles from the vapour phase almost doubling the initial number of GB particles), and changed its shape, assuming an elongated form. Eventually, the equilibrated number of particles of this $T^* = 0.53$ nanodroplet was $N \approx 47,000$, and the elongated aggregate was $90 \sigma_0$ in height and $60 \sigma_0$ in width, which in real units corresponds to a droplet with axes ≈ 45 nm and ≈ 30 nm long. The density of the surrounding vapour was $\langle \rho^* \rangle_{vap} \approx 0.00135$.

The organisation of the mesogenic particles inside the aggregate remained nematic during all stages of the equilibration process, and from the longitudinal section in Figure 1 we see that the nematic director spontaneously aligned with respect to the longest (*i.e.* principal inertia) axis.

By visual inspection one finds that the nanodroplet has a shape more similar to an ellipsoid with blunted apexes rather than to a spindle-shaped tactoid. Furthermore, by using a colour coding to map the orientation of each

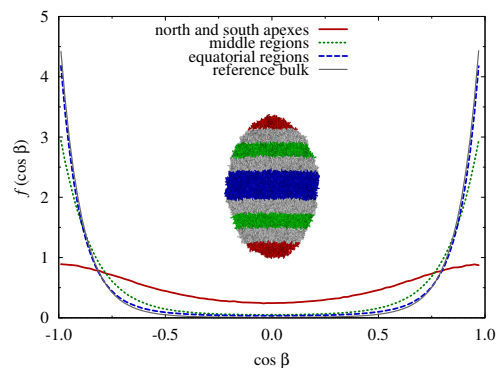


Fig. 6 Average orientational probability distributions $f_{\text{drop}}(\cos \beta)$ for the GB particles of the various flat layers sliced out perpendicularly to the droplet director (*i.e.* the principal inertia axis) as shown in the inset pictorial representation: apexes (red, continuous curve, $\langle P_2 \rangle = 0.18 \pm 0.04$), middle (green, dotted curve, $\langle P_2 \rangle = 0.55 \pm 0.04$), and equatorial (blue, dashed curve, $\langle P_2 \rangle = 0.63 \pm 0.03$). The distribution $f_{\text{bulk}}(\cos \beta)$ for a reference nematic bulk at dimensionless temperature $T^* = 0.53$ and pressure $\langle P^* \rangle = 0.00061$ is also plotted (grey, continuous curve, $\langle P_2 \rangle = 0.68 \pm 0.03$).

GB particle with respect to the overall inertia axis of the nanodroplet it is quite evident that the director field has a bipolar symmetry (see Figure 1).

To quantitatively assess the attainment of an equilibrium state we have monitored the time evolution of the populations of both vapour and condensed particles. The MD trajectory has been analysed and the GB particles sorted out into the two coexisting phases by means of a neighbour counting algorithm (*i.e.* based on the local number density value). In particular, for each MD configuration we have calculated the histogram of the population of GB particles with a given number of GB ellipsoids within a $5 \sigma_0$ cutoff distance from their centre (see Figure 2). Using these spherical sampling regions it was possible to identify and map the vapour, condensed, and interface particles during the entire simulation run. As threshold values we have chosen a number of neighbours lower than 40 for the vapour, and higher than 145 for the nematic bulk: these values have been estimated from the average values of density for the vapour and the nematic phases at these thermodynamic conditions⁶⁷. The interface particles are consequently those with a number of neighbours in the cutoff sphere between 40 and 145. As an example, we show in Figure 3 a cross-section of the equilibrated nanodroplet displaying the results of this mapping procedure with the chosen threshold values. The average thickness of the interface layer of the nematic nanodroplet is approximately $3 \sigma_0$, correspond-

ing to the length of one GB particle, similar to what was found by an hyperbolic tangent fit of the density profile across the interface in⁶⁰. In Figure 4 we also report the initial evolution of these populations during the nanodroplet equilibration. We see that at very short times the number of nematic and that of interface particles undergo a fast complementary variation, the former ones increasing and the latter ones decreasing in time. During this period the reorganisation from cubic to an elongated shape also takes place. After 2.5×10^6 time steps the population of the interface particles levels off to a stable plateau value, while the condensation of vapour particles steadily continues, even though at a slowing down rate until after 5×10^6 time steps (the end of the MD simulation run) the populations of the droplet and the vapour have reached the stable stationary state described before for the equilibrated sample.

A first step towards the characterisation of the nanodroplet structural features is the computation of the instantaneous order parameter $P_2(t)$ measuring the orientational order of the long molecular axes along the mesophase director \mathbf{n} . For a definition of orientational order parameters see *e.g.* ref.⁸⁶. Using the principal inertia axis of the nanodroplet as the overall nematic director we see in Figure 5 that the instantaneous overall order parameter $P_2(t)$ equilibrates after approximately 2.5×10^6 time steps (*i.e.* $\approx 1.5 \mu\text{s}$) and levels to a value slightly smaller than 0.6. This behaviour, as observed for the population of the interface, corresponds to the initial rounding of corners and edges for the cubic nucleus towards first a globular and then an elongated shape (with the associated formation of two apical defects in the director field), In a bulk sample the previous order parameter value would indicate a medium degree of orientational ordering. However, this seems deceiving since a much higher local $P_2(t)$ would be expected on the basis of a visual inspection of the snapshot in Figure 1. This indicates that due to the intrinsic shape anisotropy of the droplet, and the presence of a curved interface, the standard algorithm used to calculate the order parameter in uniform bulk systems is quite inadequate for our purpose. This is especially true in the apical regions where the local director field departs from a cylindrical symmetry and develops instead a radial distribution, with a topological point defect (boojum) at each of the apexes.

4 Simulation results

Using a qualitative argument, the stability of the elongated organisations for nematic droplet of 10^4 – 10^5 GB particles can be explained^{28,37} in terms of the competition between orientational and elastic effects arising from

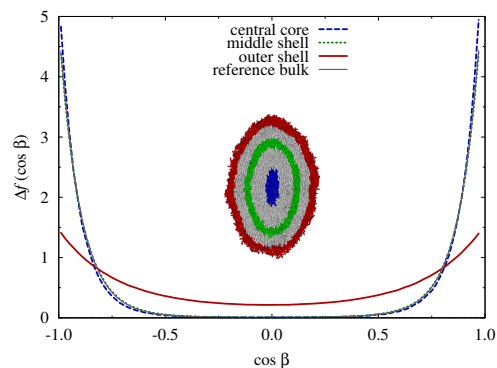


Fig. 7 Average orientational probability distributions $f(\cos \beta)$ of concentric regions of the droplet (*i.e.* onion-like shells) as shown in the inset pictorial representation: central core (blue, dashed curve, $\langle P_2 \rangle = 0.70 \pm 0.03$), middle (green, dotted curve, $\langle P_2 \rangle = 0.67 \pm 0.03$), and outer (red, continuous curve $\langle P_2 \rangle = 0.27 \pm 0.04$) shells. To improve the statistics the core and middle regions have been obtained by considering the particles belonging to pairs of adjacent concentric shells, namely (1, 2), and (7, 8) obtained with the procedure described in the text. See figure 6 for details.

the anisotropic potential, which unfavours any local distortion of an otherwise uniform director field, and eventually prevails over the surface tension which would favour instead structures with minimal surface area.

Given the non-uniform nature of our droplet–vapour system, some specific methodology has been developed. In particular, we have investigated the ordering inside the droplet and structural changes on moving from the core to the surface. A possible strategy to characterise the orientational structure of a nanodroplet would be that of partitioning it into smaller regions (typically flat layers or concentric shells) and then compute local order parameter values. However, this approach comes out to be not sensitive enough because, apart for the apical zones, the differences in the orientational distributions of the layers/shells are smoothed out, if not completely lost, during the averaging process, and all local order parameter values become similar within their statistical uncertainty (which is proportional to the inverse square root of the population of each partition, and as such very unfavourable in our case). To avoid this technical problem we have computed instead the (average) histograms of the local angular distributions. These measure the probability each molecule in a certain region has of assuming a certain orientation $\cos \beta_i$ with respect to the overall director which is practically superimposable with the principal axis of the inertia tensor of the droplet.

The positional mapping of the nematic particles has

been performed using two different approaches: the first assigning them to a certain number of flat layers sliced out perpendicularly to the director and symmetrically distributed with respect to the equator (see Figure 6–A); the second one to onion-like concentric shells (see Figure 7–A). The former particle labelling was performed after aligning the nanodroplet (*i.e.* the eigenvector associated to the smallest eigenvalue of the inertia tensor) with the laboratory Z axis, and then sorting the nematic particles, according to their z_i coordinate, into 10 layers of thickness $\approx 9 \sigma_0$. The latter mapping was obtained instead by recursively applying to the list of nematic particles the algorithm devised to identify vapour, interface, and nematic regions. After each iteration, the particles identified as interfacial ones were labelled as belonging to a new shell and removed from the list; the mapping process was then repeated until all nematic particles were labelled. Using this prescription twelve concentric shells per droplet have been obtained. We have averaged the angular distributions over 1,000 independent and well equilibrated MD configurations at $T^* = 0.53$ collected in the final part of the simulation run every 1,000 time steps. The average orientational distributions $f_{\text{drop}}(\cos \beta)$, and the one $f_{\text{bulk}}(\cos \beta)$ for a bulk nematic phase of $N = 27,000$ GB particles at temperature $T^* = 0.53$ and pressure $\langle P^* \rangle = 0.00061$ (*i.e.* a state point close to the nematic–vapour phase transition) are reported in Figures 6–B and 7–B.

From the local orientational distributions obtained via a mapping of the positions into flat layers sliced out perpendicularly to the director (Figure 6–B) we see that the difference of orientational order with respect to a bulk phase is smaller in the equatorial region of the droplet, while it steadily increases when approaching the two apical boojums. Moreover, the branches of these distributions, corresponding to opposite northern ($+z$) and southern ($-z$) regions, are essentially superimposable as expected on symmetry arguments, so the director distribution is invariant upon reflection with respect to an equatorial plane normal to the principal inertia axis. Moving from the essentially undistorted equatorial regions towards the apical defects the orientational ordering progressively decreases and the orientational distribution $f(\cos \beta)$ becomes more and more flat.

We can also observe from the histograms of Figure 7–B the influence of the distance from the interfacial region and the apical defects on the internal nematic order. While the central core and the middle shells have orientational distributions which are essentially indistinguishable from that of the nematic bulk, the outer shells which directly sample the nematic/vapour interface and the local surface curvature affect the orientation of the local

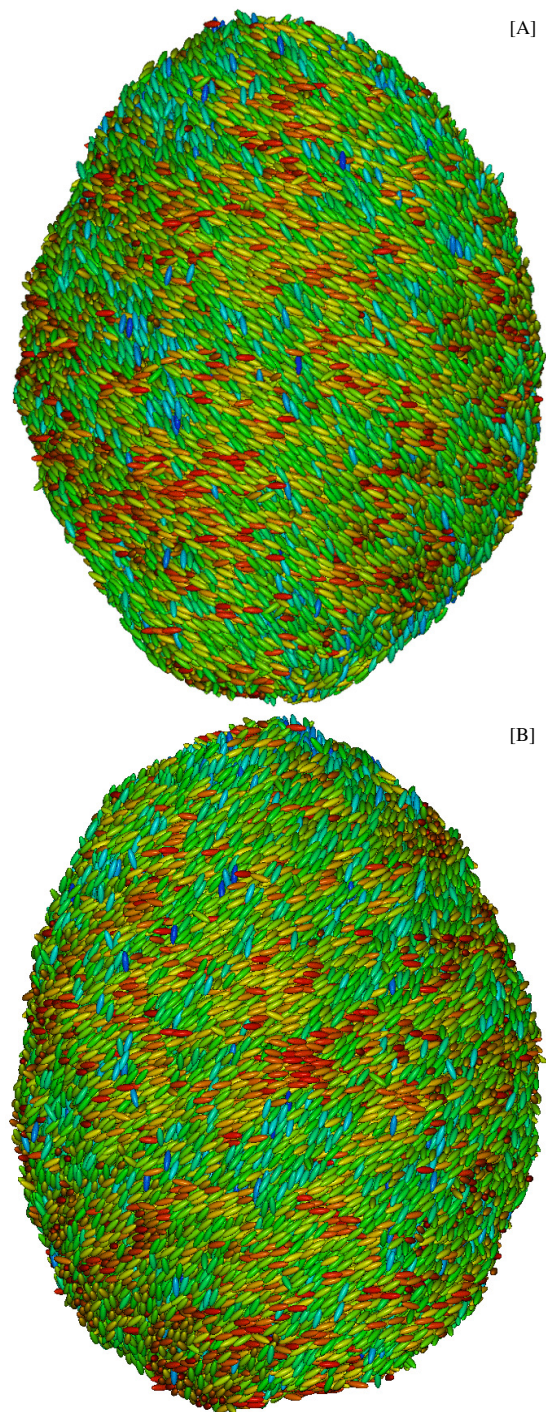


Fig. 8 Lateral views of the final configurations of two nematic freely-suspended droplets of $N \approx 100,000$ GB particles spontaneously evolved into two opposite left- (plate A) and right-handed (plate B) chiral structures. To help in the visualisation, the outer $3 \sigma_0$ thick interface layer and the gas phase particles have been removed from both nanodroplets and the core nematic GB particles are shown using a colour coding giving the orientation with respect to the overall director (see palette in Figure 1–B).

nematic director for a depth of $\approx 12 \sigma_0$, corresponding to four molecular lengths.

In the $N \approx 47,000$ particles nanodroplet (and smaller ones studied in preliminary investigations not reported here for brevity) we never observed any significant departure of the director field from a bipolar distribution with cylindrical (uniaxial) symmetry with respect to the inertia axis. However, as we already discussed in the Introduction, first Williams²⁷ and later van der Schoot and coworkers^{35,36} theoretically predicted that freely-suspended droplets of nanometric sizes formed by achiral nematogens could spontaneously break the symmetry of the director field into a helical distribution of local orientations when certain conditions for elastic constant, anchoring strength and droplet volume are met.

In particular it is expected that when the splay elastic constant of the nematic is sufficiently large with respect to twist (*i.e.*, $\gamma_{22} = K_{22}/K_{11}$ sufficiently small) a spontaneous transition from an untwisted (achiral) to a twisted (chiral) nematic field in nematic nanodroplets could occur by converting part of the splay elastic energy (concentrated at the apexes) into a twist deformation. Unfortunately, there are no previous theoretical calculations or computer simulations of the elastic constants for the specific GB parameterisation used here, and due to the large fluctuations of the observables conventionally used for this type of calculations^{39–45} we did not attempt to compute them here.

Although we can not check *a priori* if the requirements raised by the previous models are met by our GB systems, we have directly assessed by MD computer experiments the nematic field behaviour for nanodroplets with an increasing number of GB particles trying to see if the achiral small droplets become chiral as their size increases.

Using the procedure described before, we have prepared six cubic nematic samples at temperature $T^* = 0.53$ and number of GB particles ranging from $N \approx 50,000$ up to $N \approx 110,000$ (with increments of 10,000 ellipsoids) carved from an equilibrated three-dimensional bulk system at the same temperature. To prevent any bias towards the formation of a specific helicity (chirality), the initial translational and angular velocities were randomly sampled from uniform distributions with amplitude corresponding to the desired temperature, and the sample-wide values of the linear or angular momenta, have been subsequently set to zero. The empty volume surrounding the initial nematic cubic core has then been filled in all experiments with a GB vapour of density $\rho_{vap}^* = 0.00135$, corresponding to the equilibrium value previously obtained. With this prescription no significant condensation or evaporation of GB particles took place during the equilibration, allowing a rather precise

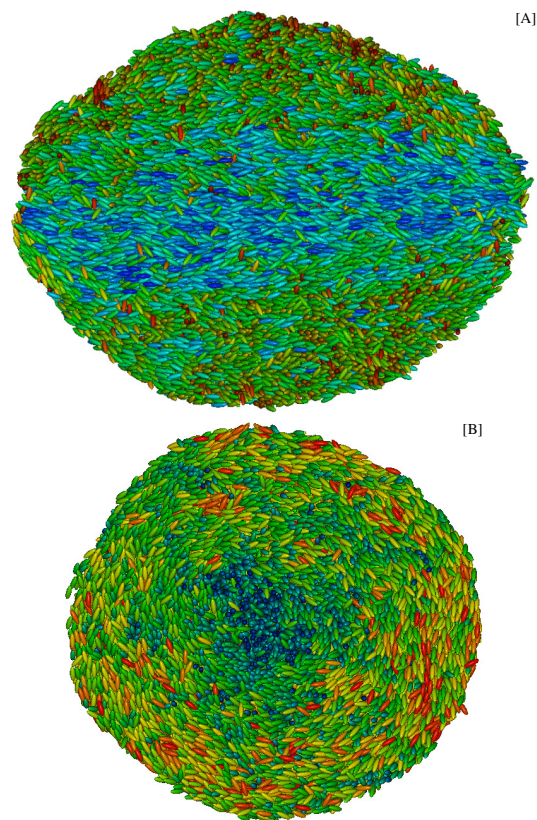


Fig. 9 Longitudinal (plate A) and transversal (plate B) views of the cross sections of the $N \approx 100,000$ GB particles right-handed chiral nanodroplet of Figure 8–B.

control of the overall nanodroplet number of particles. Each system has then been thoroughly equilibrated for at least 5×10^6 time steps at temperature $T^* = 0.53$, in order to achieve a stationary state. For the larger samples we actually did observe the spontaneous evolution of the nematic director field of the prolate nanodroplets into chirally twisted distributions very similar to the loxodromes observed by Tortora and Lavrentovich³⁷. For instance, for the $N \approx 100,000$ particles nanodroplet of Figure 8–B an equilibrium right-handed pattern of local surface directors has been observed. By repeating this MD experiment and starting from a new configuration with the same positions and orientations for the GB particles (but with different sets of initial velocities), and zero total linear and angular momenta, we observed instead the spontaneous development of a left-handed twist in the nematic director field (see Figure 8–A). Notice that to improve the graphical rendering of the surface helical pattern we excluded from the visualisation both vapour and interface GB particles.

To complete this phenomenological characterisation we

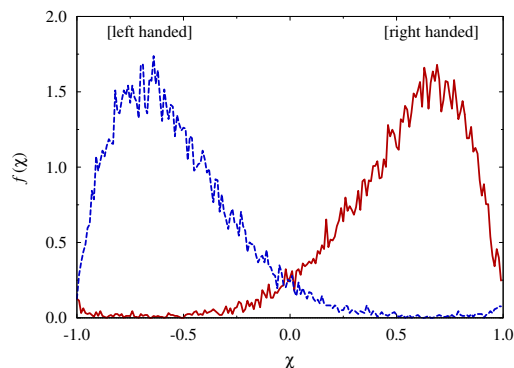


Fig. 10 The probability distributions of the chirality index χ for the nematic core from two equilibrated $N \approx 100,000$ GB particles nanodroplets at $T^* = 0.53$ and $t^* = 1 \times 10^4$ of Figure 8 spontaneously evolved into a left-handed (blue, dashed curve, with 78,845 nematic core particles) and a right-handed (red, continuous curve, with 78,895 nematic core particles) helical distribution of surface orientations after starting from two equivalent achiral initial configurations.

report in Figure 9 a pair of snapshots showing the longitudinal and transversal cross-sections for the twisted right-handed chiral nanodroplet of Figure 8-B. By colour coding the particles according to their orientation with respect to the principal rotation axis it is possible to see that the twist deformation is larger close to the equatorial surface, while the uniaxial nematic field is fairly unperturbed in the interior cylindrical region near the inertia axis and which is crossing the nanodroplet from one apex to the other. Regarding the deviation from the theoretical “slender” shape of a tactoid, our chiral nanodroplets appear to be rather “blunted” with a fairly large splay angle at the apexes. This suggests that in our GB nematic the elastic energy is minimised by transferring part of the contribution arising from the splay deformation into a twisted director distribution, and that the effect of surface tension of our GB model is not small compared to the elastic one.

To quantitatively analyse the extent of these twisted distributions of orientations we have computed the histograms of the probability of observing a suitable pseudoscalar single-particle chirality index χ_i defined as the value of the scalar triple product between three unit vectors

$$\chi_i = \mathbf{n} \cdot (\mathbf{r}_{\perp,i} \times \mathbf{z}_{+,i}), \quad (2)$$

where \mathbf{n} is the overall nematic director, while $\mathbf{r}_{\perp,i}$ and $\mathbf{z}_{+,i}$ are respectively the orientation of the radial position vector in cylindrical coordinates for each GB particle i ,

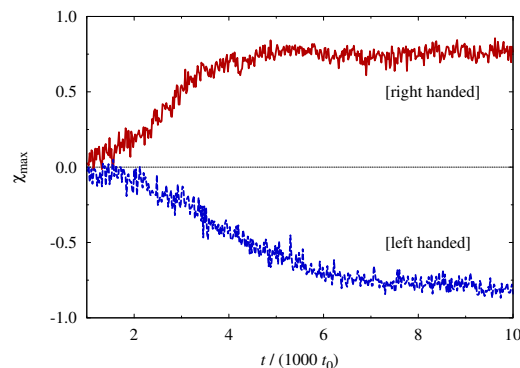


Fig. 11 The time evolution of the mode χ_{\max} for the single-particle chirality index χ_i distributions for two nematic nanodroplets of Figure 10. The early-stage noisy values for $t < 1,000 t_0$ corresponding to the relaxation from a cubic to an elongated shape of the aggregate have not been plotted.

and the unit vector giving the orientation of the long molecular axis along the laboratory \mathbf{Z} axis. The last unit vector allows to take into account the cylindrical symmetry of the GB ellipsoids while avoiding cancellation effects arising from the otherwise equally probable $+\mathbf{z}_i$ and $-\mathbf{z}_i$ orientations of the long GB molecular axes. In practice, for each pair of unit vectors $\pm\mathbf{z}_i$ we have chosen those $\mathbf{z}_{+,i}$ giving a positive $\mathbf{z}_i \cdot \mathbf{Z}$ scalar product (*i.e.* those \mathbf{z}_i unit vectors with a positive Z component).

In order to reduce the statistical noise arising from the low-structured interface region, the chirality analyses have been performed discarding the GB particles in the outermost interface layer (of thickness $\approx 3 \sigma_0$), and considering only the remaining N_χ nematic core particles. In Figure 10 we plot the distribution of the single-particle chirality indexes χ_i for the final configurations for the $N \approx 100,000$ GB particles nanodroplets with opposite handedness of the helical director field (corresponding to the snapshots of Figures 8 and 9). Both chiral distributions present a well defined peak χ_{\max} , a tail extending also in the region of opposite values of χ_i with respect to the mode, and exchange each other under reflection with respect to the $\chi_i = 0$ axis.

We have also followed the spontaneous symmetry breaking dynamics for both the right- and left-handed nanodroplets sampling (every 1,000 time steps) the mode χ_{\max} of the chirality index distributions for the $N \approx 100,000$ GB particles nanodroplets and plotted their time evolution (see Figure 11) during the early stages of the equilibration process. Notice that these plots start at 5×10^5 time steps when the initially cubic samples have already evolved into prolate nanodroplets for which the

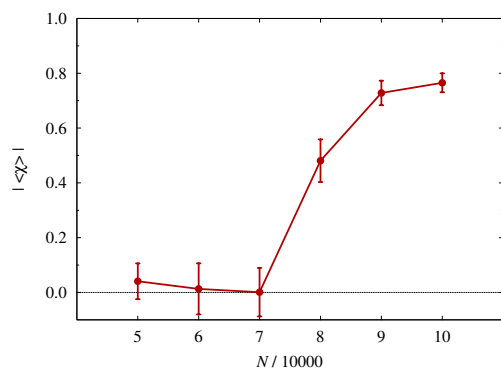


Fig. 12 The absolute value of the average chirality index $|\langle\chi\rangle|$ for nematic nanodroplets at $T^* = 0.53$ with various number of GB particles from $N = 50,000$ to $110,000$. The arithmetic mean values have been computed with respect to the last 10^6 time steps of the MD trajectory and by sampling a configuration every 1,000 time steps. All simulations have started from an achiral starting configurations.

chirality index can be actually computed. Similar analyses have also been performed for the six nanodroplets with number of particles ranging between $N \approx 50,000$ and $N \approx 110,000$ GB particles with the aim of identifying a lower limiting number of aggregate particles for which a twisted nematic director field becomes more stable than the cylindrical bipolar one.

We see that the nanodroplet chirality is established after a few ns and then remains stable in time. From each histogram of the χ_i values the overall chirality index for a nanodroplet is computed as an arithmetic mean with respect to the N_χ core particles of the configuration, defined earlier on, as $\chi = (\sum_i^{N_\chi} \chi_i) / N_\chi$. For right-handed nanodroplets we have measured $\chi > 0$ while for left-handed director fields $\chi < 0$. Furthermore, to compare the results from the MD simulations of various number of particles we have calculated the absolute value of the average chirality index $|\langle\chi\rangle|$ over the final 1×10^6 time steps by sampling one MD configuration every 1,000 time steps. The values reported in Figure 12 show a sharp increase of $|\langle\chi\rangle|$ around a critical number of $N \approx 80,000$ particles, while for smaller samples $|\langle\chi\rangle|$ was zero within the estimated statistical uncertainties. Since the largest nanodroplet we studied was formed by $N \approx 110,000$ GB particles, we can not make any prediction about the upper number of particles boundary for which the director distribution in the nematic nanodroplet becomes again achiral. Incidentally, we also notice that the sheer equilibration time necessary to equilibrate these chiral nematic droplets does not increase linearly with the number of aggregate particles. A possible explanation lies in the fact that as the droplets

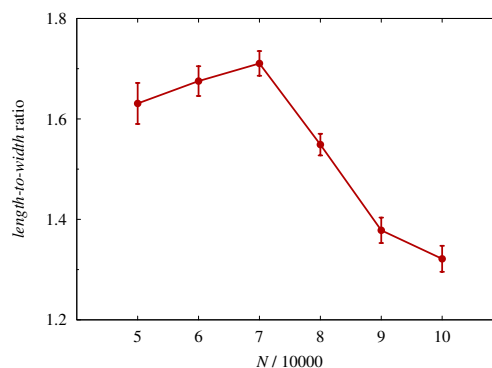


Fig. 13 The average *length-to-width* ratios for the nematic nanodroplets of Figure 12.

become larger in the early stages of the simulation the two tips can develop director distributions with opposite chiralities and the prevailing of one distribution over the other comes out to be a rather slow process compared to the equilibration of achiral structures.

The comparison of the *length-to-width* aspect ratios of our nematic nanodroplets with those measured in³⁷ reveals that while the experimental values of this shape anisotropy parameter give for all those sessile droplets length a constant *length-to-width* ratio ≈ 1.3 (and correspondingly a *width-to-depth* ratio ≈ 1), in our freely suspended MD droplets we observe instead two essentially linear regimes (see Figure 13) in this ratio. For the droplets smaller than $N = 80,000$ the shape anisotropy increases with the number of particles, and the nematic aggregates become progressively more elongated and spindle-like. However, in correspondence of the appearance of a chiral surface director field for $N \geq 80,000$, this trend is reversed, and the *length-to-width* ratio decreases with droplet size.

In most cases these ratios hint that for our samples sizes (corresponding to droplets of size below 100 nm) the weight the elastic constants have in determining the overall shape anisotropy is dominant over that of the surface tension. This latter contribution becomes instead more relevant in the case of our model off-lattice droplets for sizes $N > 100,000$ GB particles.

The structures observed for increasing sizes of the nematic nanodroplets can be compared against the theoretical predictions for the shape and the director field distribution^{27,35,36} based on a free energy expansion for the droplets. In particular, in their papers Prinsen and van der Schoot^{35,36} predicted of an extremely narrow stability region in the elastic-constant surface-tension space for nematic tactoids with twisted director distribution to exist. However, our observation by molecular dynam-

ics computer simulations of these organisations is rather serendipitous since we did not perform a prior search in model pair potential and its parameter space for a system fulfilling the aforementioned requirements. So, it could be the case that these chiral organisations for nematic nanodroplet are easier to come by than expected on the basis of these theoretical arguments.

5 Conclusions

We have presented the results of MD computer simulations at coarse-grained level of freely-suspended nematic nanodroplets in equilibrium with their vapour formed by a number of elongated 3 : 1 GB particles ranging from $N \approx 50,000$ to $N \approx 100,000$, and corresponding to droplet lengths in the 50–100 nm range. For the smaller size nanodroplets the physics of these nematic systems appears to be dominated by the anisotropic elastic properties of the nematic fluid, rather than its surface tension and for aggregates formed by a number of GB particles $N < 80,000$ the freely-suspended droplets evolve into elongated shapes with a symmetric bipolar director field and two boojum defects at the apexes. The *length-to-width* ratio for these droplets increases linearly with the number of particles and the overall organisation is qualitatively compatible with that of a tactoid. For droplets formed by a number of GB particles $N \geq 80,000$ we have found a spontaneous formation of chiral surface distributions of the molecular orientations. This change of director field is accompanied by a departure from the tactoid shape and the formation of a “flattened” or “blunted” shape, and the *length-to-width* ratio decreases with increasing number of particles, while chirality remains, at least up to our largest droplet size of 110,000 particles. Since the continuum models provide fairly restrictive ranges of elastic constants and surface tensions for observing chiral nematic droplets we argue that on the nanoscale this kind of organisation may be more common than what would be expected on the grounds of these theoretical predictions.

Acknowledgements

We thank MIUR PRIN national project “*Novel ordered systems for high response molecular devices*” (2009N5JH4F) for financial support, and the CINECA computing centre for computer time.

References

- 1 P.-G. de Gennes, F. Brochard-Wyart and D. Quéré, *Capillarity and wetting phenomena: drops, bubbles, pearls, waves*, Springer

- Verlag, 2004.
- 2 S. R. Forrest, *Nature*, 2004, **428**, 911–918.
- 3 S. Biswas, S. Gawande, V. Bromberg and Y. Sun, *J. Sol. Energy Eng.*, 2010, **132**, 021010.1–7.
- 4 M. O’Neill and S. M. Kelly, *Adv. Mater.*, 2011, **23**, 566–584.
- 5 P. S. Drzaic, *Liquid Crystal Dispersions*, World Scientific, 1995.
- 6 G. P. Crawford and S. Žumer, *Liquid Crystals in Complex Geometries*, Taylor and Francis, 1996, pp. 1–19.
- 7 O. Tongcher, R. Sigel and K. Landfester, *Langmuir*, 2006, **22**, 4504–4511.
- 8 A. Méndez-Vilas, A. B. Jódar-Reyes and M. L. González-Martin, *Small*, 2009, **5**, 1366–1390.
- 9 Y. Bai and N. L. Abbott, *Langmuir*, 2011, **27**, 5719–5738.
- 10 V. J. Alino, J. Pang and K. L. Yang, *Langmuir*, 2011, **27**, 11784–11789.
- 11 A. M. Lowe and N. L. Abbott, *Chem. Mater.*, 2012, **24**, 746–758.
- 12 A. Rapini and M. Papoular, *J. Phys. Colloques*, 1969, **30**, C4–54–C4–56.
- 13 A. Pizzirusso, R. Berardi, L. Muccioli, M. Ricci and C. Zannoni, *Chem. Sci.*, 2012, **3**, 573–579.
- 14 J. D. Bernal and I. Fankuchen, *J. Gen. Physiol.*, 1941, **25**, 111–146.
- 15 H. Zocher, *Z. Anorg. Allg. Chem.*, 1925, **147**, 91–110.
- 16 A. S. Sonin, *J. Mater. Chem.*, 1998, **8**, 2557–2574.
- 17 A. V. Kaznacheev, M. M. Bogdanov and S. A. Taraskin, *J. Exp. Theor. Phys.*, 2002, **95**, 57–63.
- 18 A. Kaznacheev, M. Bogdanov and A. Sonin, *J. Exp. Theor. Phys.*, 2003, **97**, 1159–1167.
- 19 Z. Dogic and S. Fraden, *Phil. Trans. R. Soc. Lond. A*, 2001, **359**, 997–1015.
- 20 N. D. Mermin, *Physics Today*, 1981, **34**, 46–53.
- 21 P. S. Drzaic, *Liq. Cryst.*, 1999, **26**, 623–627.
- 22 T. J. Bunning, L. V. Natarajan, V. P. Tondiglia and R. L. Sutherland, *Annu. Rev. Mater. Sci.*, 2000, **30**, 83–115.
- 23 C. Bacchiocchi, I. Miglioli, A. Arcioni, I. Vecchi, K. Rai, A. Fontecchio and C. Zannoni, *J. Phys. Chem. B*, 2009, **113**, 5391–5402.
- 24 J. K. Gupta, S. Sivakumar, F. Caruso and N. L. Abbott, *Angew. Chem. Int. Ed.*, 2009, **48**, 1652–1655.
- 25 C. Herring, *Phys. Rev.*, 1951, **82**, 87–93.
- 26 S. Chandrasekhar, *Mol. Cryst. Liq. Cryst.*, 1966, **2**, 71–80.
- 27 R. D. Williams, *J. Phys. A: Math. Gen.*, 1986, **19**, 3211–3222.
- 28 W. Huang and G. F. Tuthill, *Phys. Rev. E*, 1994, **49**, 570–574.
- 29 E. G. Virga, *Variational theories for liquid crystals*, Chapman and Hall / CRC, 1994.
- 30 G. Barbero and L. R. Evangelista, *Adsorption Phenomena and Anchoring Energy in Nematic Liquid Crystals*, Taylor & Francis, 2006.
- 31 G. E. Volovik and O. D. Lavrentovich, *J. Exp. Theor. Phys.*, 1983, **58**, 1159–1166.
- 32 V. L. El’nikova, *J. Supercond. Nov. Magn.*, 2008, **21**, 473–478.
- 33 O. D. Lavrentovich and V. V. Sergan, *Nuovo Cimento D*, 1990, **12**, 1219–1222.
- 34 F. Xu, H. S. Kitzerow and P. P. Crooker, *Phys. Rev. E*, 1994, **49**, 3061–3068.
- 35 P. Prinsen and P. van der Schoot, *J. Phys.: Condens. Matter*, 2004, **16**, 8835–8850.
- 36 P. Prinsen and P. van der Schoot, *Phys. Rev. E*, 2003, **68**, 021701.1–11.
- 37 L. Tortora and O. D. Lavrentovich, *Proc. Nat. Acad. Sci.*, 2011, **108**, 5163–5168.

- 38 C. Chiccoli, O. D. Lavrentovich, P. Pasini and C. Zannoni, *Phys. Rev. Lett.*, 1997, **79**, 4401–4404.
- 39 M. P. Allen and D. Frenkel, *Phys. Rev. A*, 1988, **37**, 1813–1816.
- 40 M. P. Allen and D. Frenkel, *Phys. Rev. A*, 1990, **42**, 3641–3641.
- 41 B. Tjpto-Margo, G. T. Evans, M. P. Allen and D. Frenkel, *J. Phys. Chem.*, 1992, **96**, 3942–3948.
- 42 M. P. Allen, M. A. Warren, M. R. Wilson, A. Sauron and W. Smith, *J. Chem. Phys.*, 1996, **105**, 2850–2858.
- 43 J. Stelzer, M. A. Bates, L. Longa and G. R. Luckhurst, *J. Chem. Phys.*, 1997, **107**, 7483–7492.
- 44 N. H. Phuong, G. Germano and F. Schmid, *J. Chem. Phys.*, 2001, **115**, 7227–7234.
- 45 H. Steuer and S. Hess, *Phys. Rev. Lett.*, 2005, **94**, 027802.1–4.
- 46 J. Stelzer, R. Berardi and C. Zannoni, *Chem. Phys. Lett.*, 1999, **299**, 9–16.
- 47 J. R. Errington and D. A. Kofke, *J. Chem. Phys.*, 2007, **127**, 174709.1–12.
- 48 G. J. Gloor, G. Jackson, F. J. Blas and E. de Miguel, *J. Chem. Phys.*, 2005, **123**, 134703.1–19.
- 49 J. G. Sampayo, A. Malijevský, E. A. Müller, E. de Miguel and G. Jackson, *J. Chem. Phys.*, 2010, **132**, 141101.1–4.
- 50 B. J. Block, S. K. Das, M. Oettel, P. Virnau and K. Binder, *J. Chem. Phys.*, 2010, **133**, 154702.1–12.
- 51 S. K. Das and K. Binder, *Europhys. Lett.*, 2010, **92**, 26006.1–4.
- 52 C. Chiccoli, P. Pasini, F. Semeria and C. Zannoni, *Phys. Lett. A*, 1990, **150**, 311–314.
- 53 J. Dzubiella, M. Schmidt and H. Löwen, *Phys. Rev. E*, 2000, **62**, 5081–5091.
- 54 S. I. Hernández, J. A. Moreno-Razo, A. Ramírez-Hernández, E. Díaz-Herrera, J. P. Hernández-Ortiz and J. J. de Pablo, *Soft Matter*, 2012, **8**, 1443–1450.
- 55 C. Chiccoli, P. Pasini, F. Semeria and C. Zannoni, *Phys. Lett. A*, 1990, **150**, 311–314.
- 56 E. Berggren, C. Zannoni, C. Chiccoli, P. Pasini and F. Semeria, *Phys. Rev. E*, 1994, **50**, 2929–2939.
- 57 C. Chiccoli, Y. Lansac, P. Pasini, J. Stelzer and C. Zannoni, *Mol. Cryst. Liq. Cryst.*, 2002, **372**, 157–165.
- 58 M. A. Bates, *Chem. Phys. Lett.*, 2003, **368**, 87–93.
- 59 Y. K. Levine and A. Polimeno, *Eur. Phys. J. E*, 2007, **23**, 13–23.
- 60 A. P. J. Emerson, S. Faetti and C. Zannoni, *Chem. Phys. Lett.*, 1997, **271**, 241–246.
- 61 Y. Trukhina and T. Schilling, *Phys. Rev. E*, 2008, **77**, 011701.1–7.
- 62 J. K. Gupta, J. S. Zimmerman, J. J. de Pablo, F. Caruso and N. L. Abbott, *Langmuir*, 2009, **25**, 9016–9024.
- 63 J. A. Moreno-Razo, E. J. Sambriski, N. L. Abbott, J. P. Hernandez-Ortiz and J. J. de Pablo, *Nature*, 2012, **485**, 86–89.
- 64 M. Tsige, M. P. Mahajan, C. Rosenblatt and P. L. Taylor, *Phys. Rev. E*, 1999, **60**, 638–644.
- 65 G. Tiberio, L. Muccioli, R. Berardi and C. Zannoni, *ChemPhysChem*, 2009, **10**, 125–136.
- 66 J. G. Gay and B. J. Berne, *J. Chem. Phys.*, 1981, **74**, 3316–3319.
- 67 E. de Miguel, E. M. del Rio, J. T. Brown and M. P. Allen, *J. Chem. Phys.*, 1996, **105**, 4234–4249.
- 68 E. de Miguel, L. F. Rull, M. K. Chalam and K. E. Gubbins, *Mol. Phys.*, 1991, **74**, 405–424.
- 69 E. de Miguel and C. Vega, *J. Chem. Phys.*, 2002, **117**, 6313–6322.
- 70 R. Berardi, A. P. J. Emerson and C. Zannoni, *J. Chem. Soc. Faraday Trans.*, 1993, **89**, 4069–4078.
- 71 C. Zannoni, *J. Mater. Chem.*, 2001, **11**, 2637–2646.
- 72 M. P. Allen, G. T. Evans, D. Frenkel and B. M. Mulder, *Adv. Chem. Phys.*, 1993, **86**, 1–166.
- 73 P. Bolhuis and D. Frenkel, *J. Chem. Phys.*, 1997, **106**, 666–687.
- 74 R. Berardi, A. Costantini, L. Muccioli, S. Orlandi and C. Zannoni, *J. Chem. Phys.*, 2007, **126**, 044905.1–8.
- 75 W. M. Brown, M. K. Petersen, S. J. Plimpton and G. S. Grest, *J. Chem. Phys.*, 2009, **130**, 044901.1–7.
- 76 Y. Trukhina, S. Jungblut, P. van der Schoot and T. Schilling, *J. Chem. Phys.*, 2009, **130**, 164513.1–7.
- 77 L. F. Rull, J. M. Romero-Enrique and A. Fernandez-Nieves, *J. Chem. Phys.*, 2012, **137**, 034505.1–7.
- 78 R. Berardi, C. Fava and C. Zannoni, *Chem. Phys. Lett.*, 1995, **236**, 462–468.
- 79 R. Berardi, C. Fava and C. Zannoni, *Chem. Phys. Lett.*, 1998, **297**, 8–14.
- 80 R. Everaers and M. R. Ejtehadi, *Phys. Rev. E*, 2003, **67**, 041710.
- 81 X. Zheng and P. Palfy-Muhoray, *Phys. Rev. E*, 2007, **75**, 061709.1–6.
- 82 H. J. C. Berendsen, J. P. M. Postma, W. F. van Gunsteren, A. D. Nola and J. R. Haak, *J. Chem. Phys.*, 1984, **81**, 3684–3690.
- 83 S. J. Plimpton, *J. Comp. Phys.*, 1995, **117**, 1–19.
- 84 S. J. Plimpton, URL <http://lammps.sandia.gov/>, 2008.
- 85 J. Nickolls, I. Buck, M. Garland and K. Skadron, *Queue*, 2008, **6**, 40–53.
- 86 C. Zannoni, *Nuclear Magnetic Resonance of Liquid Crystals*, Reidel, Dordrecht, The Netherlands, 1985, ch. 1, pp. 1–34.